Coupling of Rotation and Catalysis in F$_1$-ATPase Revealed by Single-Molecule Imaging and Manipulation

Kengo Adachi,[1] Kazuhiro Oiwa,[2] Takayuki Nishizaka,[3] Shou Furuike,[1] Hiroyuki Noji,[4] Hiroyasu Itoh,[5] Masasuke Yoshida,[6,7] and Kazuhiko Kinosita, Jr.[1,*]

[1] Department of Physics, Faculty of Science and Engineering, Waseda University, Shinjuku-ku, Tokyo 169-8555, Japan
[2] Kobe Advanced Research Center, National Institute of Information and Communications Technology, Nishi-ku, Kobe 651-2492, Japan
[3] Department of Physics, Gakushuin University, Toshima-ku, Tokyo 171-8588, Japan
[4] The Institute of Scientific and Industrial Research, Osaka University, Ibaragi, Osaka 567-0047, Japan
[5] Tsukuba Research Laboratory, Hamamatsu Photonics KK, and CREST "Creation and Application of Soft Nano-Machine, Hyperfunctional Molecular Machine" Team 13, Tokodai, Tsukuba 300-2635, Japan
[6] ATP System Project, Exploratory Research for Advanced Technology (ERATO), Midori-ku, Yokohama 226-0026, Japan
[7] Chemical Resources Laboratory, Tokyo Institute of Technology, Midori-ku, Yokohama 226-8503, Japan
*Correspondence: kazuhiko@waseda.jp
DOI 10.1016/j.cell.2007.05.020

SUMMARY

F$_1$-ATPase is a rotary molecular motor that proceeds in 120° steps, each driven by ATP hydrolysis. How the chemical reactions that occur in three catalytic sites are coupled to mechanical rotation is the central question. Here, we show by high-speed imaging of rotation in single molecules of F$_1$ that phosphate release drives the last 40° of the 120° step, and that the 40° rotation accompanies reduction of the affinity for phosphate. We also show, by single-molecule imaging of a fluorescent ATP analog Cy3-ATP while F$_1$ is forced to rotate slowly, that release of Cy3-ADP occurs at ~240° after it is bound as Cy3-ATP at 0°. This and other results suggest that the affinity for ADP also decreases with rotation, and thus ADP release contributes part of energy for rotation. Together with previous results, the coupling scheme is now basically complete.

INTRODUCTION

F$_1$-ATPase is a rotary molecular motor in which a central γ subunit rotates against hexagonally arranged subunits α$_3$β$_3$ (Abrahams et al., 1994; Boyer and Kohlbrenner, 1981; Kinosita et al., 2000, 2004; Noji et al., 1997; Weber and Senior, 2000; Yoshida et al., 2001). Three β subunits, each hosting a catalytic site, hydrolyze ATP sequentially to power the rotation of the γ subunit. It is a reversible molecular machine in that, when γ is rotated in the reverse direction by an external force, ATP is synthesized in the catalytic sites (Itoh et al., 2004). The reversal achieved by manipulation of the γ angle alone implies a γ-dictator mechanism: the rotary angle of γ determines which of the chemical reactions is to occur in each catalytic site, binding/release of ADP and inorganic phosphate (Pi), synthesis/hydrolysis of ATP, and release/binding of ATP (Kinosita et al., 2004). During rotation driven by ATP hydrolysis, the three catalytic sites (and the three β subunits) will cooperate by communication through the γ angle.

A major task that remains is to establish the actual coupling scheme between the γ rotation and chemical reactions. Here we propose the scheme in Figures 1A and 1B (or 1C) for ATP-driven rotation; in principle, ATP synthesis by reverse rotation would follow the same scheme in reverse. Previously we have shown that rotation of F$_1$-ATPase occurs in steps of 120°, each driven by hydrolysis of one ATP molecule (Adachi et al., 2000; Yasuda et al., 1998). At submillisecond time resolution, the 120° step is further resolved into 80°–90° and 40°–30° substeps. Initially we reported the substep amplitudes as 90° and 30° (Yasuda et al., 2001), but subsequent studies (Hirono-Hara et al., 2001; Nishizaka et al., 2004; Shimabukuro et al., 2003) indicated that they are closer to 80° and 40°. Hereafter, we adopt the latter values, although experimental precision does not warrant absolute distinction and a possibility remains that a third small substep may exist between the two (Kinosita et al., 2004). The 80° substep is driven by ATP binding, and the 40° substep by release of ADP or Pi (Yasuda et al., 2001). After a 80° substep, γ dwells on 80° for ~2 ms, during which two ~1 ms reactions take place (Yasuda et al., 2001). One of the reactions at 80° has been identified as ATP hydrolysis (Shimabukuro et al., 2003). The ATP that is hydrolyzed there is one that was bound 200° ago (Figure 1B; Nishizaka et al., 2004): an ATP molecule that is bound at 0° will be hydrolyzed after γ rotates for 120° + 80°.
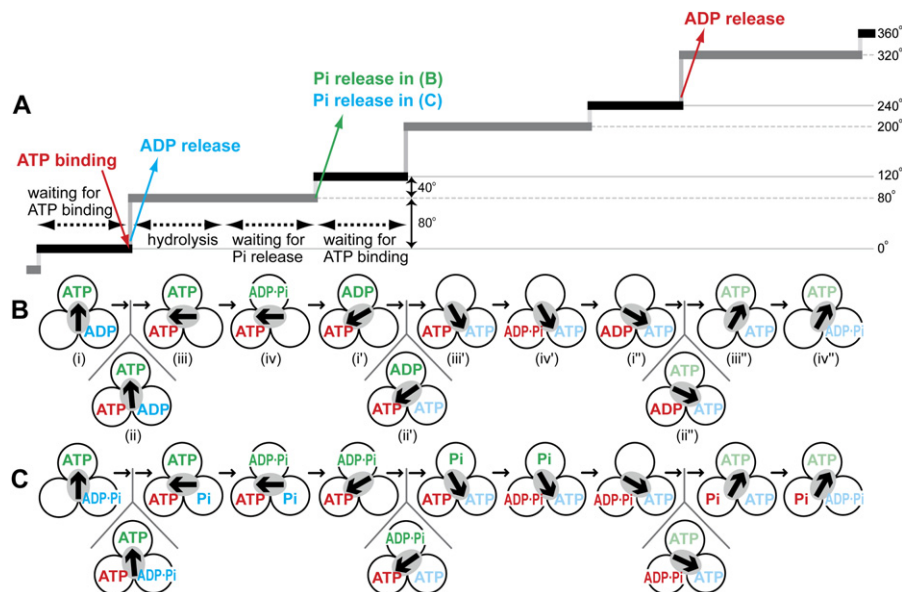
Figure 1. Proposed Coupling Scheme

(A) Schematic time course of stepping rotation. Vertical axis is the rotary angle of γ, and the horizontal axis time. Colored events take place in the catalytic site shown in the same color in (B) or (C).

(B) Corresponding nucleotide states in the three catalytic sites. The three circles represent three β subunits that each hosts a catalytic site. The central gray ellipsoid represents the γ subunit, the thick arrow showing its orientation; the twelve o'clock position in (i) corresponds to 0° in (A). Molecular species derived from the same ATP molecule are shown in the same color. Small arrows show the progress in this major reaction pathway; the configurations (ii), (ii'), and (ii'') shown below the major path represent the instant immediately after ATP binding, i.e., the start of a 80° substep.

(C) An alternative scheme in which Pi release lags behind ADP release.

Here, we show by high-speed imaging of γ rotation that the other of the two ~1 ms reactions at 80° is Pi release, and that the Pi release drives the last 40° substep. We also show that ADP is released at 240° after it is bound as ATP at 0°, by direct observation of the binding and release of a fluorescent ATP analog 2′-O-Cy3-EDA-ATP (Oiwa et al., 2003), hereafter referred to as Cy3-ATP, in a single molecule of F_1-ATPase. These two findings complete the basic scheme as shown in Figure 1B, with a possible alternative in Figure 1C. A similar scheme has been proposed (Weber and Senior, 2000).

RESULTS

Timing of Phosphate Release

In this study, we used the minimal subcomplex of F_1-ATPase that is active in hydrolysis and rotation, composed of $\alpha_3\beta_3\gamma$ subunits. The subcomplex, which we refer to as F_1 in this paper, was derived from thermophilic *Bacillus* PS3 and has been modified such that it has only two cysteine residues at the protruding portion of γ and that each β has a histidine tag at the amino terminus (α-C193S, β-His$_{10}$ at amino terminus, γ-S107C, γ-I210C). Because these modifications are minor, we regard this mutant as wild-type. We immobilized the F_1 molecules on a glass surface functionalized with Ni-NTA that would bind the introduced histidines on β. To observe rotation,

we biotinylated the cysteines on γ and attached a 40 nm gold bead through streptavidin-biotin linkages. Because the bead was small, the rate of rotation would be limited by chemical reactions rather than viscous friction against the bead, and thus we should be able to resolve the 80° and 40° substeps.

To see whether it is the release of Pi or ADP that induces the 40° substep, we added phosphate to the buffer for rotation assay. In the absence of Pi and at 2 mM ATP, we observed 80° dwells averaging ~2 ms, as before (Yasuda et al., 2001), whereas ATP-waiting dwells at 0° (and multiples of 120°) were short and mostly unresolved at the temporal resolution of 0.125 ms (black in Figure 2A). Addition of Pi increased the dwell time at 80°, without much effect at 0° (red and magenta in Figure 2A), suggesting that Pi release triggers 40° substeps. At 20 μM ATP, near the Michaelis-Menten constant K_m for unloaded rotation and hydrolysis (Yasuda et al., 2001), both 0° and 80° dwells were clearly resolved, with similar dwell times in the absence of Pi (black in Figure 2B). Addition of Pi at 20 μM ATP prolonged both dwells (red and magenta in Figure 2B). KCl also prolonged the 0° dwell, but not the 80° dwell (green in Figure 2B), suggesting that only the prolongation of the 80° dwell is specific to phosphate. We further examined the effect of divalent anions, inorganic sulfate and organic succinate (Figures 2C–2F). The plots versus ionic strength (Figures 2E and 2F) show that both 0° and 80° dwells are sensitive
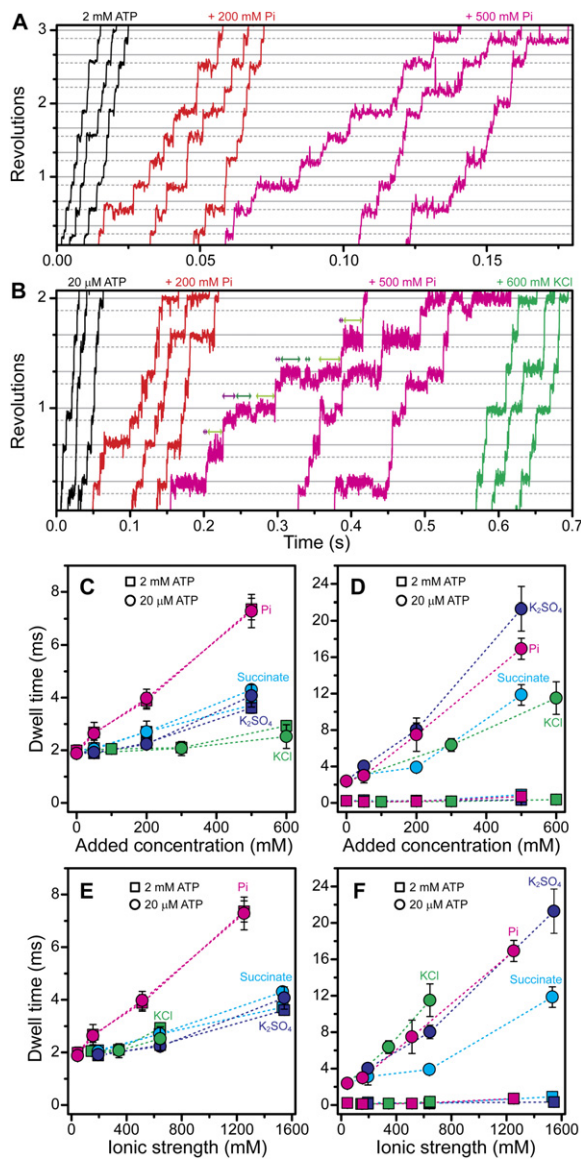
Figure 2. Effect of Phosphate on Substep Kinetics

(A and B) Time courses of stepping rotation of a 40 nm gold bead at indicated [ATP] with addition of Pi or KCl as indicated; black curves, no addition. Curves with the same color are continuous, shifted to save space. Horizontal solid lines are separated by 120°, showing ATP-waiting angles, and dotted lines are drawn 40° below. For arrows, see legend to Figure 3.

(C and D) Effect of indicated ions on the dwell time at 80° (C) and 0° (D). In records of >15 continuous revolutions, all dwells on the dotted lines as in (A) or (B) were counted as 80° dwells, and those on solid lines as 0° dwells; 0° dwells from which a 40° backward substep occurred were discounted. Dwell times were measured between the ends of preceding and following substeps; the ends were identified as the first point, within the fluctuation level, of the next dwell; 0° dwells at 2 mM ATP were mostly absent and given a value of 0 s. Each symbol shows a mean ± SEM over 2–5 molecules.

(E and F) Data in (C) and (D) plotted against the ionic strength (see Experimental Procedures).

to the ionic strength, the 80° dwell to a much lesser extent, and that the effect of Pi on the 80° dwell is outstanding among others, even against its kin sulfate. Thus we conclude that the 40° substep terminating a 80° dwell is triggered by the release of phosphate. The unusually high Pi concentration ([Pi]) needed to retard the 40° substep is due to rapid rotation of γ in the 40° substep, which takes less than our resolution of 0.125 ms: Pi has to rebind before γ rotates (see below for quantitative analysis).

We further propose that Pi release not only triggers the 40° substep, possibly by initiating a next reaction(s) that causes the 40° substep, but is the reaction that is directly coupled to the 40° rotation. If Pi release is the direct cause, rebinding of Pi after a 40° substep should lead to reversal of the substep. We indeed observed frequent reversals at 500 mM Pi, as seen in magenta lines in Figure 2B. When driving force for rotation originates from Pi release, that rotation should accompany a decrease in the affinity of the catalytic site for Pi (Kinosita et al., 2004). This explains why 500 mM Pi was required to observe frequent backward substeps, as analyzed in detail below.

Kinetics and Energetics of Phosphate Release

In this section, we determine from experiments the rate constants in Figure 3A and thereby estimate the free-energy differences among the four configurations. We consider the free energy G of the system composed of F_1 and medium as the function of the chemical state S of F_1 (we denote the states before and after Pi release as $S = F_1 \cdot ADP \cdot Pi$ and $F_1 \cdot ADP$; the analysis below applies to Figure 1C as well), the γ angle θ (conformation of F_1 for the given chemical state), and [Pi] (Kinosita et al., 2004). Although θ is a continuous variable, here we adopt the simple two-conformation diagram in Figure 3A and neglect intermediate conformations ($80° < \theta < 120°$), which would not be populated significantly because 40° rotation is fast.

We denote the angle-dependent rates for Pi release and rebinding by $k_{off}^{Pi}(\theta)$ and $k_{on}^{Pi}(\theta)$, respectively, where $\theta = 80°$ or 120°. Then, $\Delta G_{bind}(\theta)$, per F_1 molecule, for Pi binding at θ (magenta to green in Figure 3A) is given by

$$\Delta G_{bind}(\theta) \equiv G(F_1 \cdot ADP \cdot Pi; \theta, [Pi]) - G(F_1 \cdot ADP; \theta, [Pi])$$
$$= k_B T \ln K_d^{Pi}(\theta) - k_B T \ln[Pi] \qquad (1)$$

where $K_d^{Pi}(\theta) = k_{off}^{Pi}(\theta)/k_{on}^{Pi}(\theta)$ is the angle-dependent dissociation constant and $k_B T = 4.1 \, pN \cdot nm$ the thermal energy at room temperature. Rotary rates k^+ and k^- are related to $\Delta G_{rot}(S)$, the change in conformational energy upon rotation in the given chemical state S, or the mechanical work needed for the rotation, by

$$\Delta G_{rot}(S) \equiv G(S; 120°, [Pi]) - G(S; 80°, [Pi])$$
$$= k_B T \ln\{k^-(S)/k^+(S)\} \qquad (2)$$

Previous studies have indicated that the work done in 120° rotation amounts to 80–90 pN·nm, and that the
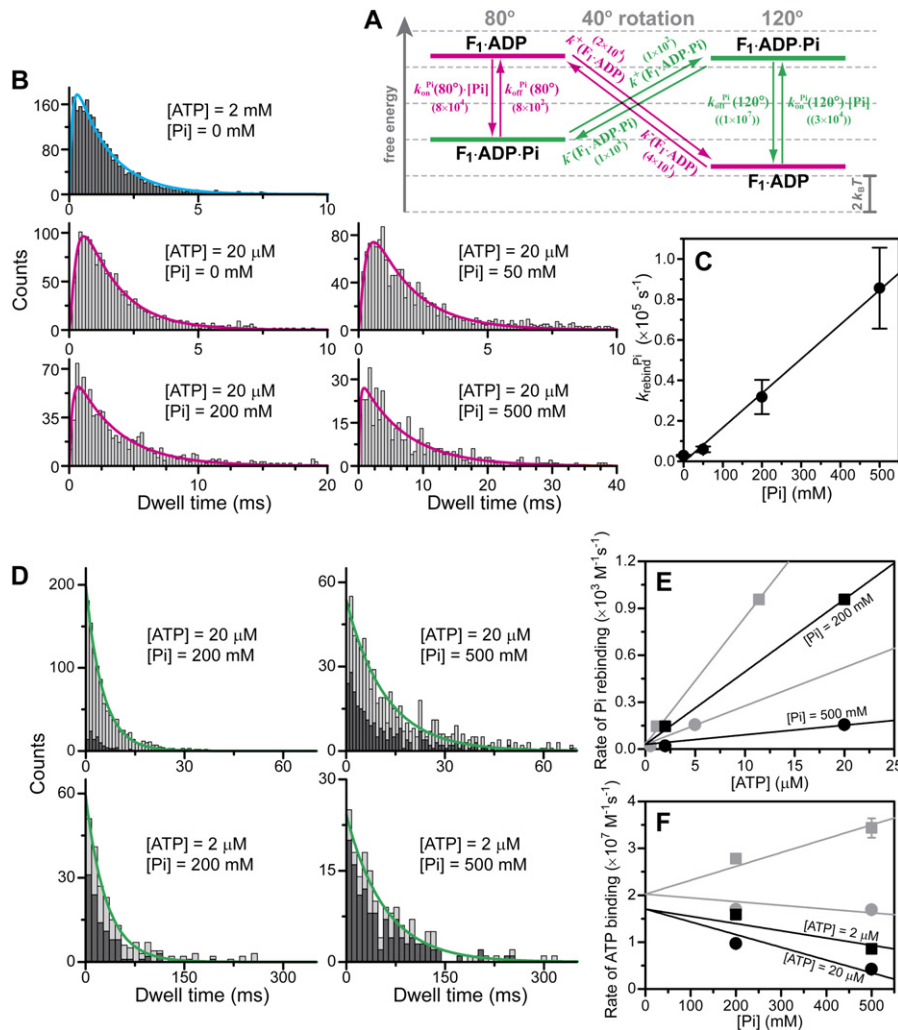
Figure 3. Kinetics of Phosphate Release and Rebinding

(A) Free-energy diagram for the 40° substep from 80° to 120°. Arrows indicate rate constants; experimental values, in /s, are shown in parentheses for [Pi] of 500 mM; values in double parentheses are mere guess, except that their ratio is experimental.

(B) Histograms of dwell times at 80°. Dwells were identified and measured as in purple arrows in Figure 2B (also see Figure 2 legend). Each histogram was from five molecules (three at 50 mM Pi). Cyan line shows fit with constant×{exp($-k_1t$) − exp($-k_2t$)}. Magenta lines show a global fit to the four histograms with Equation 8: R^2, the coefficient of determination, is 0.993, 0.970, 0.953, and 0.912 for the four individual histograms (0.972 for all); global fits in which one each of the four histogram was omitted gave parameter values within 10% of those in total fit.

(C) Pi dependence of the first-order Pi rebinding rate at 80° obtained from the global fit in (B). Error bars show SEM.

(D) Histograms of dwell times at 120° (equivalent with 0°), each from 2–5 molecules. Dark gray, dwells terminated by a backward substep, i.e., between 80° → 120° and 120° → 80° substeps (dark green arrows in Figure 2B); light gray, all dwells including those terminated by a forward substep, i.e., between 80° → 120° and 120° → 200° substeps (yellow-green arrows in Figure 2B), and those shown in dark gray. Green lines are single-exponential fits to each light gray histogram.

(E and F) The apparent second-order rate of Pi rebinding (E) and ATP binding (F) at 120° obtained from fits in (D). Gray symbols, [MgATP] corrected for chelation of Mg by Pi (see Experimental Procedures). Errors (SEM) are smaller than the symbols, except for an error bar in (F). Lines are linear fits with a common y intercept.

energy-conversion efficiency may reach ~100% (Yasuda et al., 1998). Because the torque of this motor is nearly constant over rotary angles (Kinosita et al., 2000, 2004), the work in the 40° (or possibly 30°) substep is given simply as {(40°–30°)/120°} × (80–90) pN·nm = (20–30) pN·nm ≈25 pN·nm. The high efficiency suggests that

this work is nearly equal to the available conformational energy (Kinosita et al., 2004):

$$\Delta G_{rot}(F_1 \cdot ADP) \approx -25 \text{ pN·nm} \tag{3}$$

In the Pi-bound state, the 80° conformation must be stable, and thus

$$\Delta G_{rot}(F_1 \cdot ADP \cdot Pi) > 0 \qquad (4)$$

Consistency requires
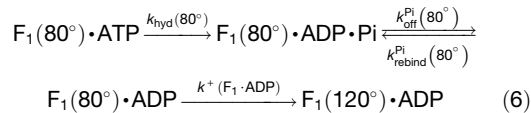
$$-\Delta G_{bind}(80°) + \Delta G_{rot}(F_1 \cdot ADP) + \Delta G_{bind}(120°)$$
$$- \Delta G_{rot}(F_1 \cdot ADP \cdot Pi) = 0$$

or

$$k_{off}^{Pi}(80°) \times k^+(F_1 \cdot ADP) \times k_{on}^{Pi}(120°) \times k^-(F_1 \cdot ADP \cdot Pi)$$
$$= k_{off}^{Pi}(120°) \times k^-(F_1 \cdot ADP) \times k_{on}^{Pi}(80°)$$
$$\times k^+(F_1 \cdot ADP \cdot Pi) \qquad (5)$$

Now we determine the eight rate constants in Figure 3A. We first analyze the events at 80°. Figure 3B shows histograms of dwell times at 80°. Reactions that determine the duration of a 80° dwell are

$$F_1(80°) \cdot ATP \xrightarrow{k_{hyd}(80°)} F_1(80°) \cdot ADP \cdot Pi \underset{k_{rebind}^{Pi}(80°)}{\overset{k_{off}^{Pi}(80°)}{\rightleftharpoons}}$$

$$F_1(80°) \cdot ADP \xrightarrow{k^+(F_1 \cdot ADP)} F_1(120°) \cdot ADP \qquad (6)$$

where $k_{hyd}(80°)$ is the rate of ATP hydrolysis, and $k_{rebind}^{Pi}(80°)$ represents the first-order rate $k_{on}^{Pi}(80°)[Pi]$; we have assumed that the rate of thermal process $k^+(F_1 \cdot ADP \cdot Pi)$ is negligible, as justified below. Simultaneous, or global, fit to all four histograms at [ATP] = 20 μM in Figure 3B with this scheme (see Experimental Procedures), with all parameters in common except for $k_{rebind}^{Pi}(80°)$, gave $k_{hyd}(80°) = (4.1 \pm 0.1) \times 10^3 \ s^{-1}$, $k_{off}^{Pi}(80°) = (8.4 \pm 0.1) \times 10^2 \ s^{-1}$, $k^+(F_1 \cdot ADP) = (1.8 \pm 0.1) \times 10^4 \ s^{-1}$, and $k_{rebind}^{Pi}(80°)$ values shown in Figure 3C (errors in this paper are SEM, standard error of a mean, unless stated otherwise). Though let free, $k_{rebind}^{Pi}(80°)$ was found to be proportional to [Pi] (Figure 3C), as expected, and the slope gave the second-order rate $k_{on}^{Pi}(80°)$ of $(1.7 \pm 0.1) \times 10^5 \ M^{-1}s^{-1}$. This rate is two orders of magnitude smaller than the rate of ATP binding at 0° (Yasuda et al., 2001), suggesting that the Pi-release site at 80° is less open than the site waiting for ATP at 0°. The rate $k^-(F_1 \cdot ADP)$ for thermally agitated rotation in the reverse direction is calculated from Equation 3 as $4.0 \times 10^1 \ s^{-1}$. The dissociation constant for Pi at 80°, $K_d^{Pi}(80°) = k_{off}^{Pi}(80°)/k_{on}^{Pi}(80°)$, is 4.9 mM, which is close to physiological [Pi]. Al-Shawi et al. (1997) have reported a similar value of ~3 mM for K_m for ATP synthesis in E. coli F_1.

Of the remaining four of the eight rate constants in Figure 3A, we set $k^-(F_1 \cdot ADP \cdot Pi) \approx 10^4 \ s^{-1}$, because the backward 40° substep was as fast as the forward substep with $k^+(F_1 \cdot ADP)$ of $1.8 \times 10^4 \ s^{-1}$. The rest were obtained from the analysis of dwells at 120° (Figure 3D), as detailed in Experimental Procedures. At this angle, a 40° backward substep driven presumably by Pi rebinding (thermal rate $k^-(F_1 \cdot ADP)$ being small) and a forward 80° substep driven by ATP binding compete with each other. The simplest scheme is

$$F_1(80°) \cdot ADP \cdot Pi \xleftarrow{k_{on}^{Pi,app} \cdot [Pi]} F_1(120°) \cdot ADP$$
$$\xrightarrow{k_{on}^{ATP}(120°) \cdot [ATP]} F_1(200°) \cdot ADP \cdot ATP \qquad (7)$$
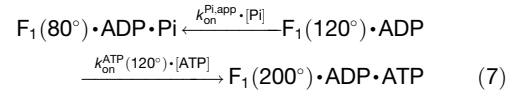
where $k_{on}^{Pi,app}(120°)$ and $k_{on}^{ATP}(120°)$ are apparent binding rates defined by this simplified scheme. This scheme predicts an exponential dwell-time distribution, exp(-kt). Fitting each histogram in Figure 3D yielded four values of $k = k_{on}^{Pi,app}[Pi] + k_{on}^{ATP}[ATP]$, which we plot as k/[Pi] in Figure 3E and k/[ATP] in Figure 3F. The intercepts at [ATP] = 0 and [Pi] = 0 respectively gave $k_{on}^{Pi,app}(120°) = (4.4 \pm 2.5) \times 10^1 \ M^{-1}s^{-1}$ and $k_{on}^{ATP}(120°) = (2.0 \pm 0.3) \times 10^7 \ M^{-1}s^{-1}$, the latter being consistent with the previous estimate (Yasuda et al., 2001). From $k_{on}^{Pi,app}(120°)$ together with other constraints, we obtain two possible sets of parameters (Experimental Procedures): (i) $k^+(F_1 \cdot ADP \cdot Pi) \approx 10^2 \ s^{-1}$, and $K_d^{Pi}(120°) = k_{off}^{Pi}(120°)/k_{on}^{Pi}(120°) \approx 2 \times 10^2 \ M$. The last two rates could not be determined except for the ratio, and we make an arbitrary choice of $k_{off}^{Pi}(120°) = 10^7 \ s^{-1}$ and $k_{on}^{Pi}(120°) = 5 \times 10^4 \ M^{-1}s^{-1}$. (ii) $k^+(F_1 \cdot ADP \cdot Pi) \approx 3 \times 10^2 \ s^{-1}$, $k_{off}^{Pi}(120°) \approx 3 \times 10^3 \ s^{-1}$, and $k_{on}^{Pi}(120°) \approx 4 \times 10^1 \ M^{-1}s^{-1}$, giving $K_d^{Pi}(120°) \approx 7 \times 10^1 \ M$. The two sets (i) and (ii) give similar values for $K_d^{Pi}(120°)$, 200 M or 70 M, which is >10^4 greater than $K_d^{Pi}(80°)$ of 4.9 mM; a state of F_1 where K_d is far above 1 M has been documented (Weber and Senior, 2000), though it is not clear whether it corresponds to $K_d^{Pi}(120°)$. The >10^4-fold reduction in affinity drives the 40° rotation. $\Delta G_{rot}(F_1 \cdot ADP \cdot Pi)$ in Equation 2 is 18 pN·nm in (i) and 14 pN·nm in (ii), which are indistinguishable. Both are positive, ~4 k_BT, implying that the Pi-bound state is more stable at 80° than at 120°. Because the set (ii) is only marginally possible (Experimental Procedures), we opt for (i) and show, in Figure 3A, numerical values of the rate constants at 500 mM Pi in parentheses, the two arbitrary rates in double parentheses. At different [Pi]s, the two green bars shift vertically by a same amount, according to Equation 1. At physiological [Pi] of ~5 mM, green and magenta bars at 80° nearly overlap, whereas at 120°, the green bar is above by ~11 k_BT (probability of finding bound Pi ≈ 0.00003).

Timing of ADP Release during Slow, Controlled Rotation

Having established the timing of phosphate release, we next inquire when ADP is released. Because F_1-ATPase is prone to inhibition by MgADP (Hirono-Hara et al., 2001), we could not add ADP in the medium as in the experiments with phosphate above. Instead we directly visualized the binding and release of Cy3-AT(D)P on single molecules of F_1 with total internal reflection fluorescence (TIRF) microscopy. Simultaneously, we controlled the rotation of F_1 with magnets by attaching a magnetic bead(s) to γ, while imaging the bead movement with bright-field microscopy (Figure 4A). Cy3-ATP bound to F_1 appeared as a bright spot in the fluorescence image, whereas unbound Cy3-ATP gave dim, homogeneous background because of its rapid Brownian motion in solution (Funatsu et al.,
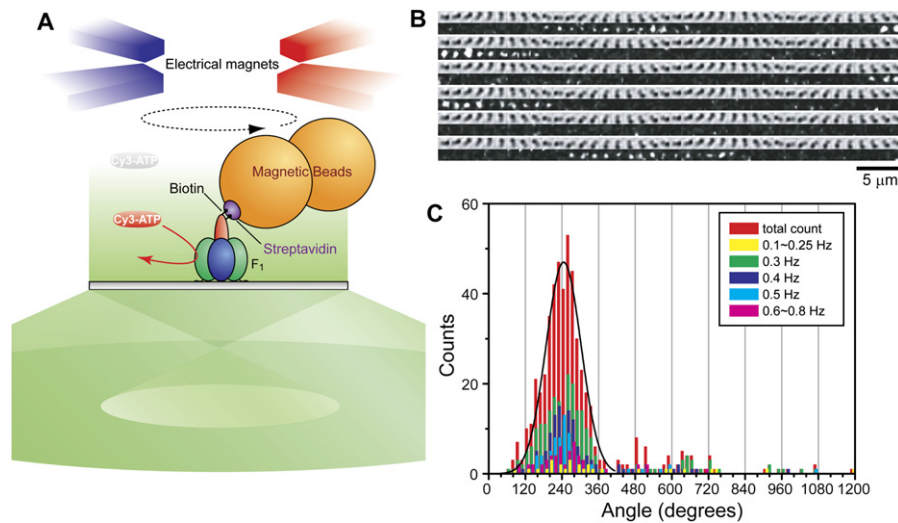
Figure 4. Angle between Binding and Release of Cy3-ATP during Controlled Rotation

(A) Experimental design for observation of Cy3-ATP binding during rotation controlled with magnets (not to scale). Cy3-ATP bound to F_1 was imaged by TIRF microscopy through the entire edge of the objective lens, and, simultaneously, rotation of magnetic beads attached to γ was observed by bright-field microscopy. Quadripolar electromagnets were mounted over the sample stage to control the magnetic beads.

(B) Sequential bright-field images, at 100-ms intervals, of magnetic beads (upper rows) and fluorescence images of single Cy3-ATP molecules (lower rows) at 100 nM Cy3-ATP and 200 nM unlabeled ATP under a rotary magnetic field at 0.5 Hz. Images have been spatially averaged over 6 × 6 pixels (1 μm = 10.2 pixels), and then averaged over 2 frames.

(C) Histogram of angles between binding and release at various rotation speeds. Events involving overlapping binding periods are excluded. Total counts for all speeds (red) are fitted by a Gaussian curve (black line) with a peak and SD of 245° ± 57° (8 molecules).

1995; Nishizaka et al., 2004). Detection of single fluorophores requires an integration time, and thus we used ordinary video cameras at 30 frames/s for the results below.

To resolve the angles of binding and release at 30 frames/s, we forced γ to rotate slowly in the hydrolysis direction at a constant speed using electromagnets (Figure 4A). The medium contained 100 nM Cy3-ATP and 200 nM ATP, and the rotary speed was lower than ~1.7 revolutions/s, time-averaged rate of rotation driven by unlabeled ATP at 200 nM. The rate of Cy3-ATP binding was about one-tenth that of unlabeled ATP (see below), and thus F_1 bound mostly unlabeled ATP and occasionally Cy3-ATP (Figure 4B). When Cy3-ATP was bound, it was released, presumably as Cy3-ADP, after 245° ± 57° (SD) of rotation, irrespective of the rotary speed (Figure 4C). If this result applies to unlabeled ATP as well, ATP that is bound at 0° will be released as ADP at ~240°, simultaneous with the binding of a third ATP (Figure 1A).

Timing of ADP Release during Stepping Rotation

We also examined the timing of Cy3-ADP release during spontaneous, uncontrolled rotation. At the video rate, resolving the release angle during stepping motion was impossible, but we hoped to distinguish whether release occurred in the first 80° or second 40° portion of a step. To resolve the substeps, we used ATP-γ-S for which the 80° dwell is extended to ~70 ms presumably because its cleavage on F_1 is slow (Shimabukuro et al., 2003). At 60 nM Cy3-ATP and 60 nM ATP-γ-S, some of the 120°

steps were clearly resolved into 80° and 40° substeps (Figure 5A). When Cy3(-ADP) was released in a resolved 120° step, the release occurred in the 80° substep, after binding of Cy3-ATP and subsequent 240° rotation (between green lines in Figure 5A). Previously we have shown that Cy3-ATP bound at 0° is released in a 120° step between 240° and 360° (Nishizaka et al., 2004), and now we show that the release occurs between 240° and 320°, consistent with the forced-rotation result above that the angle between binding and release is ~240°.

For the spontaneous rotation at 60 nM Cy3-ATP and 60 nM ATP-γ-S, we observed 297 pairs of binding and release in 23 F_1 molecules. Most were consistent with the scheme in Figure 1, but there were exceptions indicative of non-major reaction pathways. In the following statistics, we regard a 120° step to be resolved into substeps when the bead stayed at ~80° for two video frames (67 ms) or longer: otherwise the step is classified as an unresolved 120° step. We judged binding/release and a step/substep to be coincident when one was within two frames of the other. (i) Of the 297 pairs, 205 (69%) were normal without reservation, in that binding of Cy3-ATP at 0° (an ATP-waiting angle) was coincident with a 80° substep or an unresolved 120° step, and that release of Cy3 occurred in a step or 80° substep starting from 240°. Of the 205, 47 binding events were associated with a resolved substep pair, and all these bindings were in a 80° substep; 59 release events were coincident with a resolved substep, all 80° and none 40°. (ii) In 26 pairs (9%), release occurred
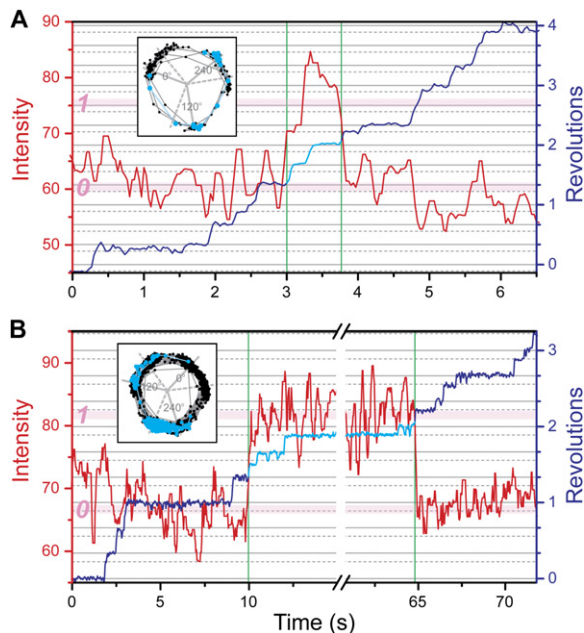
Figure 5. Binding and Release of Cy3-ATP during Spontaneous Rotation

Time courses of Cy3-ATP binding and stepping rotation. (A) Wild-type F_1 at 60 nM Cy3-ATP and 60 nM ATP-γ-S. (B) β-E190D mutant at 100 nM Cy3-ATP and 2 μM unlabeled ATP. Red curves show fluorescence intensity in a spot of 8 × 8 pixels (0.784 × 0.784 μm^2), median-filtered over 6 video frames (0.2 s) in (A) and 8 video frames in (B). Pink horizontal lines, intensity levels for the indicated number of bound Cy3-ATP molecules (see Experimental Procedures). Blue curves show rotation time courses, cyan parts between green vertical lines indicating the period when Cy3-ATP was bound. Horizontal dotted lines are 40° below the solid lines that show ATP-waiting angles. Insets, trace of the centroid of the bead image, cyan part indicating binding.

after 360° rotation or more. Most of these can be explained by successive binding of two or more Cy3-ATP molecules, and are thus considered normal. (iii) In 66 pairs (22%), binding and release angles were separated by less than 240°, or release occurred at 240° without rotation. (iiia) In 35 cases (12%) out of the 66, either binding or release was not synchronous with rotation. Possible explanations are blinking (momentary disappearance of fluorescence) or photobleaching (irreversible destruction) of Cy3 fluorophore while the F_1 still followed the reaction scheme in Figure 1. However, control experiments (see Calibration below) showed blinking was rare and average photobleaching time was 56 s, much longer than the stepping intervals of < 1 s. In addition, (iiib) the rest of 31 pairs (10%) could not be explained by the scheme in Figure 1. We think that these irregular behaviors, together with some or most of the events in iiia, represent non-major reaction pathways that we describe fully in the next section. Briefly, bound Cy3-nucleotide that had undergone 240° of rotation tended to dissociate from F_1 before the arrival of a next ATP(-γ-S) that would induce rotation toward 360°; the release at 240° was often, but not always, accompanied by a 40° backward substep to 200°, and rebinding of Cy3 after

a 40° backward substep was also observed. We consider that these irregular behaviors are peculiar to low ATP environments where thermal agitations into non-major pathways can compete with infrequent arrivals of ATP.

Substeps with ATP-γ-S were not always resolved, and therefore we attempted another experiment with a mutant F_1 (β-E190D) which cleaves ATP 100-fold slower (and binds ATP 10-fold slower) than wild-type F_1 (Shimabukuro et al., 2003). At 100 nM Cy3-ATP and 0.6 or 2 μM unlabeled ATP, most of substeps were resolved, and binding of Cy3-ATP was coincident with a 80° substep, and the release with another 80° substep after 240° rotation (Figure 5B). We observed 59 pairs of binding/release in 24 molecules. About 90% of binding was in a 80° substep, and ~70% of release was in a substep from 240° to 320°. When this mutant bound Cy3-ATP at 0°, the dwell at 200° became extremely long, averaging 33 s, indicating that cleavage of Cy3-ATP occurs at this angle and the Cy3 moiety impedes cleavage, as in another mutant (Nishizaka et al., 2004). About 25% of apparent release occurred in the midst of the long dwell at 200°, suggesting that the actual cause was photobleaching.

Site Occupancy during Stepping Rotation
The results that Cy3-ATP is released after ~240° of rotation implies that, of the three catalytic sites, two are always occupied by a nucleotide, i.e., the site occupancy remains two, except for angles around 240°. To directly confirm this, we observed rotation driven entirely by Cy3-ATP (no unlabeled ATP) while watching the fluorescence intensity to estimate the number of bound Cy3-nucleotides.

Rotation driven by Cy3-ATP alone was an order of magnitude slower than that by unlabeled ATP, with an apparent binding rate $k_{on}^{Cy3-ATP}$ of $(1.6 \pm 0.8) \times 10^6$ M^{-1}s^{-1} (Figure 6A), compared to $k_{on}^{ATP}(120°)$ of 2.0×10^7 M^{-1}s^{-1} estimated in the Pi analysis above or a previous value of 2.6×10^7 M^{-1}s^{-1} (Yasuda et al., 2001). At the low [Cy3-ATP] examined, rotation was stepwise, with exponential distribution of dwell times consistent with the $k_{on}^{Cy3-ATP}$ above (Figure 6B). We also confirmed on individual F_1 molecules that stepping angles are the same for ATP and Cy3-ATP. Cy3-ATP is thus a fairly good substrate for F_1.

At [Cy3] >200 nM, we could not resolve reliably bound Cy3 against background. With Cy3-ATP at 50, 100, and 150 nM, at most two nucleotides were bound to F_1 during rotation (Figures 6C and 6D). Regular 120° steps starting from an ATP-waiting angle occurred mostly while the site occupancy remained two (Figures 6C and 6E), as expected. During these steps, the occupancy may well have risen to three for a moment, but the change could not be detected at the video rate.

At the low [Cy3-ATP] and thus at low stepping frequencies, we observed a variety of irregular behaviors other than the normal 120° steps, as summarized in Figure 6E. Four outstanding patterns are indicated by color in Figures 6C–6E, where cyan, a stepping motion while the occupancy remains two, represents mostly, but not exclusively, the normal 120° steps. From an ATP-waiting
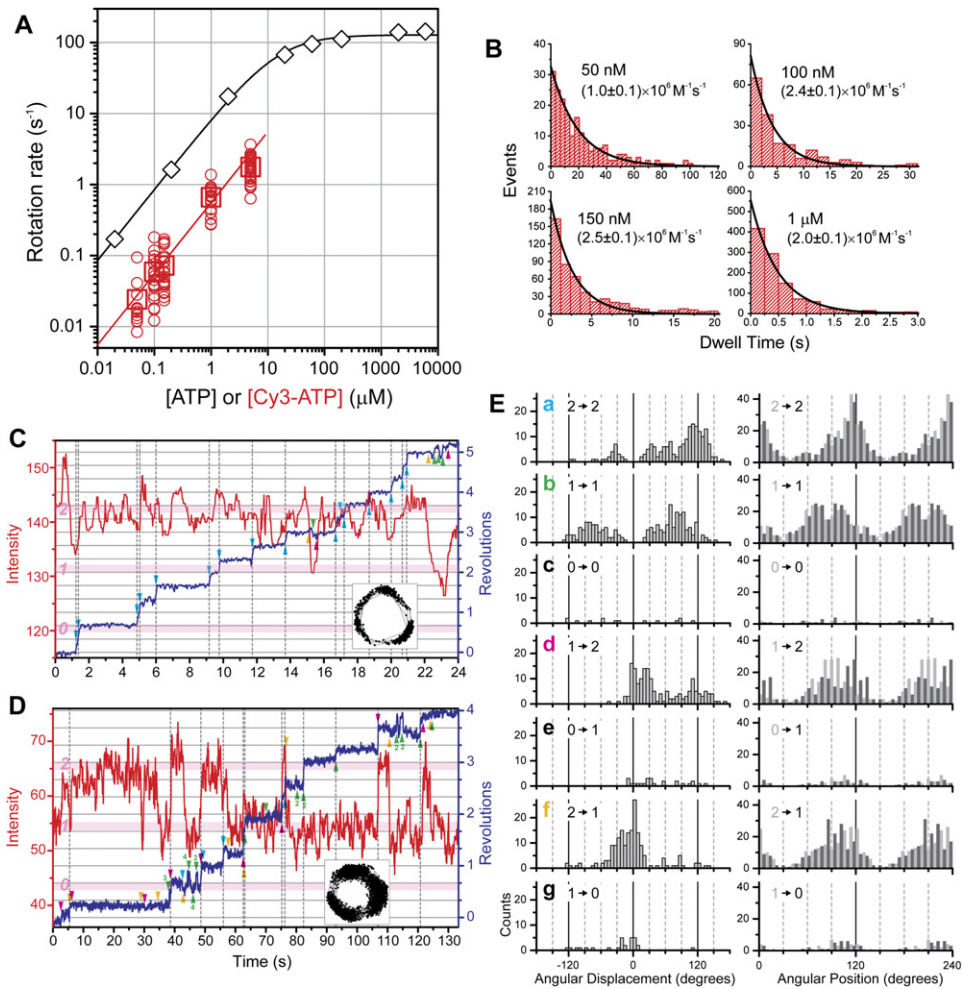
Figure 6. Rotation Driven by Cy3-ATP Alone

(A) Comparison of time-averaged rotation rates driven by Cy3-ATP and unlabeled ATP. Red circles, rotation of individual molecules driven by Cy3-ATP (12–38 molecules at each concentration) averaged over >3 continuous revolutions; red squares, average over molecules. Red line is a linear fit with $(k_{on}^{Cy3-ATP}/3) \times$ [Cy3-ATP] between 50 nM and 1 μM, where $k_{on}^{Cy3-ATP} = (1.6 \pm 0.8) \times 10^6$ M^{-1}s^{-1}. Black diamonds show published rotation rates for a 40 nm bead in unlabeled ATP (Yasuda et al., 2001), for which $k_{on}^{ATP} = (2.6 \pm 0.5) \times 10^7$ M^{-1}s^{-1}.

(B) Histograms of dwell times between 120° steps at indicated [Cy3-ATP]. Substeps and backward steps are ignored, as in the vertical dotted lines in (C) and (D). Black lines are fit with constant×exp($-k_{on}^{Cy3-ATP}$[Cy3-ATP]t); obtained rates are shown on the graphs.

(C and D) Time courses of Cy3-ATP binding and stepping rotation at 150 nM Cy3-ATP (C) and 50 nM Cy3-ATP (D). Red lines show the spot intensity (0.784 × 0.784 μm²) median-filtered over 16 video frames (0.533 s). Pink horizontal lines, intensity levels for the indicated numbers of bound Cy3-ATP. Blue lines show rotation, and vertical dotted lines mark beginnings of 120° steps which may accompany substeps in either directions in between. Insets, trace of the centroid of the bead image. Arrow heads indicate transition patterns in (E), color-coded; numbers indicate repetitions of the same transition, which are too close to each other on this time scale.

(E) Angular histograms for typical transition patterns at [Cy3-ATP] of 50 nM (3 molecules), 100 nM (8), and 150 nM (8) combined. When the number of bound Cy3-nucleotides changed, the bead angles before and after the change were registered. Or, when F$_1$ made a rotary step of amplitude >40° between plateaus of 5 frames or longer, the start and end angles as well as Cy3 number were registered. Angular changes less than 40° were also registered if it was between plateaus of >20 frames and clearly distinguishable from fluctuations. Left panels show the difference between the end and start angles. Right panels show the start (light gray) and end (dark gray) angles, modulo 120°; duplicated to 240° to show peaks around 120°, which represents an ATP-waiting angle.

angle, F$_1$ often made a backward ~40° substep accompanied by release of a Cy3-nucleotide, resulting in a one-nucleotide state at ~80° (e.g., orange arrowheads at 58 s and 111 s in Figure 6D). One-nucleotide state appeared mechanically unstable in that, while the occupancy remained one (green), F$_1$ made steps of various sizes either forward

or backward, with a tendency to come back to a ~80° position (these steps may have accompanied unresolved momentary binding of Cy3-ATP). Restoration of a two-nucleotide state by binding of Cy3-ATP (magenta) occurred mostly from a ~80° position, with four major rotation patterns categorized into two major consequences: making

a forward 40° or 160° step to reach an ATP-waiting angle to resume normal behavior, or staying at a ~80° position either without rotation or by a forward 120° step into another ~80° position. In the latter cases where F_1 remained at a ~80° position, it sometimes released and rebound a nucleotide without rotation (e.g., at 29–30 s in Figure 6D).

Similar, irregular behaviors have been observed with unlabeled ATP, at nano- to subnanomolar concentrations where stepping frequency is ~10^{-2}/s or less: occasionally F_1 makes a 40° backward step from an ATP-waiting angle and begins to step forward and backward, remaining mostly in ~80° positions separated by 120° (Sakaki et al., 2005). Our interpretation is the following: normally at higher [ATP], ADP to be released from the two-nucleotide ATP-waiting state stays on F_1 until the next ATP binds (Figures 1A and 1B). If, however, the next ATP fails to arrive for a time of the order of 10^2 s (10^1 s if the leaving nucleotide is Cy3-ADP), the ADP is spontaneously released. Once fallen into one-nucleotide state, F_1 wanders on non-major reaction pathways (toward hydrolysis direction on average, though), until ATP binds to the correct catalytic site at a correct timing to bring the F_1 back to the normal pathway. Details of the non-major pathways are yet to be studied, but it is worthwhile to note in Figure 6E that rotation tends to go in the hydrolysis direction when the site occupancy increases ($1 \rightarrow 2$ or $0 \rightarrow 1$) whereas decrease in occupancy tends to push F_1 in the synthesis direction.

Site Occupancy during Constant-Speed Rotation

To resolve the change in site occupancy during rotation, we again used magnets to force F_1 to rotate at a slow, constant speed (Figure 7). At 150 nM or 100 nM Cy3-ATP, the occupancy remained two for most of the time. Often, the occupancy dropped to one around an ATP-waiting angle, but F_1 soon bound medium Cy3-ATP to restore the occupancy to two; unlike the free stepping situation, F_1 here was forced to rotate in the forward direction, and forward rotation is expected to increase the affinity of F_1 for ATP (Yasuda et al., 2001). In other cases where the occupancy remained apparently two, quick succession of binding and release should have occurred. We did not find unambiguous sign of a three-nucleotide state lasting tens of degrees, consistent with the result in Figure 4 that ADP to be released cannot cling to F_1 much beyond 240°, at least when rotation is slow.

We often noticed a bead to rotate abruptly in the forward direction near ATP-waiting angles (vertical dotted lines in Figure 7), indicating sudden generation of forward torque. (i) In 44% (46/105) of such rapid bead displacements, the site occupancy remained two, and (ii) in 8% (8/105) apparently remained one. (iii) In 28% (29/105), the displacement was synchronous with Cy3-ATP binding (occupancy $1 \rightarrow$ 2), and (iv) in 21% (22/105) synchronous with release ($2 \rightarrow 1$). Case iii is readily explained because binding of (Cy3-)ATP is expected to produce forward torque. Case iv suggests that release of (Cy3-)ADP also produces forward torque, which is reasonable as discussed below.
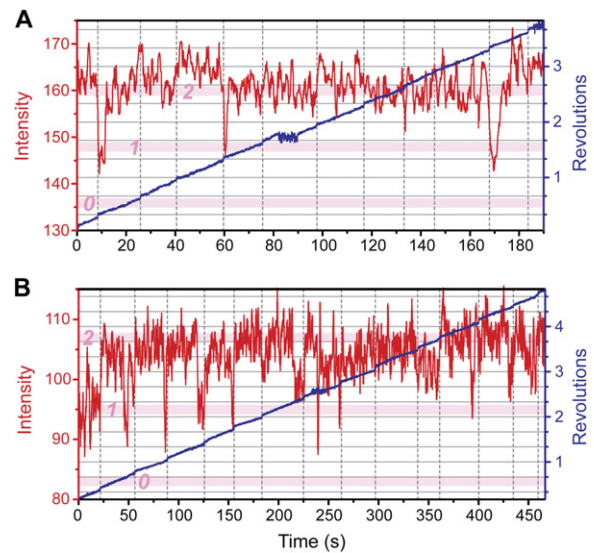
Figure 7. Site Occupancy during Controlled Rotation

Time courses of the number of bound Cy3-nucleotide and rotation under rotary magnetic field at 0.02 Hz in 150 nM Cy3-ATP (A) and at 0.01 Hz in 100 nM Cy3-ATP (B). Red curves, fluorescence intensity in a spot (0.784 × 0.784 μm²), median-filtered over 32 video frames (1.067 s). Pink horizontal lines, number of bound Cy3-nucleotide. Blue lines, bead rotation. Gray horizontal lines, ATP-waiting angles. Vertical dotted lines mark abrupt forward rotation of the beads that occurred every ~120°. The magnetic field was turned off for a while at ~82 s and 186 s in (A) and at ~234 s in (B).

Case i is a combination of cases iii and iv in that Cy3-ATP binding and Cy3-ADP release must have occurred in succession, in either order. Case ii is unexplained. Case iv, forward bead displacements accompanying ADP release, may appear at odds with the observation in the absence of magnets where the occupancy change from 2 to 1 resulted mostly in backward rotation (Figure 6E [f]). Our interpretation is that, in the one-nucleotide state arrived at by ADP release, the potential energy for γ rotation has a local maximum slightly ahead of the ATP-waiting angle: upon ADP release, γ is basically pulled backward by the $\alpha_3\beta_3$ stator, but, if an external force or thermal fluctuation moves γ past the potential maximum, the stator pushes γ forward. Without an external force, γ goes backward in most cases but occasionally goes forward by the help of thermal fluctuation. The magnets prohibit the backward motion and force γ to rotate forward, and then the $\alpha_3\beta_3$ stator adds an additional push.

DISCUSSION

The Coupling Scheme

The timings of Pi and ADP releases have been established, and the 40° substep has been shown to be driven by Pi release (Figure 1A). For ADP which remains bound for ~240°, the catalytic site that releases it is uniquely identified as the one that has bound ATP 240° ago (Figures 1B or 1C). For phosphate, however, our study leaves two

possibilities: Pi cleaved from ATP is immediately released (Figure 1B), or the release is suspended for another 120° rotation (Figure 1C). The latter is in accord with a recent crystal structure of yeast F_1 in which phosphate is located in the third, otherwise empty, catalytic site (Kabaleeswaran et al., 2006). The crystal, however, may have bound medium sulfate. A difficulty in Figure 1C is how the leaving phosphate senses its timing of release, which must be synchronous with ATP cleavage in a different, remote catalytic site; Pi release obligatorily follows ATP cleavage in Figure 1B. Another is that, prior to Pi release, the affinity for Pi is already low, with $K_d^{Pi}(80°)$ of 4.9 mM. Retaining Pi for 120° rotation after hydrolysis, which takes many seconds at low [ATP], may well pose a problem. These difficulties are highlighted in the β-E190D mutant, in which cleavage is slow, taking ~300 ms with unlabeled ATP and ~30 s with Cy3-ATP, but nevertheless phosphate tenaciously waits for the cleavage to complete. A possibility is that ATP cleavage and Pi release occur in parallel, in different sites, and γ rotation is suspended until both have taken place: Pi release may precede ATP cleavage. The kinetics for this parallel scenario is not grossly different from the sequential one. Our preference at this moment is Figure 1B, mainly because it is simple and straightforward. Under conditions where F_1 binds only one ATP molecule (uni-site catalysis), Pi is released before ADP (Masaike et al., 2002). In another motor protein myosin, force-generating Pi release occurs before ADP release (De La Cruz and Ostap, 2004).

The Pi release site aside, the scheme in Figure 1 shows how the chemical reactions in the three sites drive particular phases of rotation, which we believe represents the major reaction pathway of ATP-driven rotation at saturating, millimolar concentrations of ATP down to nanomolar. In principle, ATP synthesis by forced, reverse rotation will follow the same pathway in reverse. Synthesis is the physiological function (in animals, plants and aerobic bacteria including the thermophile) of F_1-ATPase, which is part of the ATP synthase in which the other part, a proton-driven rotary motor F_o, drives the reverse rotation of F_1 in cells (Yoshida et al., 2001). Upon reverse rotation, phosphate will be picked up from the intracellular environment at ~80°, but, there, $K_d^{Pi}(80°)$ is 4.9 mM, comparable to the physiological [Pi]. Efficient synthesis would require a K_d^{Pi} an order of magnitude smaller. Our answer is that the actual K_d^{Pi} is a steep function of the γ angle θ, increasing $>10^4$ fold over the narrow angular range of 80°–120°, whereas the $K_d^{Pi}(80°)$ of 4.9 mM represents an effective value for the two-conformation approximation in Figure 3A: in the actual, fully θ-dependent $K_d^{Pi}(\theta)$, its value at 80° is presumably below 1 mM, and thermal fluctuation of γ toward 120° will increase K_d^{Pi} to assist Pi release such that the effective K_d^{Pi} is 4.9 mM. During synthesis, an external force produced by F_o or magnets rotates γ in the reverse direction until K_d^{Pi} is reduced to a submillimolar value to ensure binding of medium Pi.

Crystal structures of F_1 solved by Walker group are all similar to each other. Our fluorescence study (Yasuda et al., 2003) has indicated that these should resemble a 80°, not 0°, conformation. The original structure (Abrahams et al., 1994) was proposed to represent the MgADP-inhibited state, where γ has been shown to be at ~80° (Hirono-Hara et al., 2001). In all these crystals but one, site occupancy is two, consistent with our scheme that ADP is released between 240° and 320°. In the structure with three sites filled (Menz et al., 2001), γ is twisted clockwise, possibly representing a state between 240° and 320°. In a two-nucleotide structure (Kagawa et al., 2004), one catalytic site (on the $β_{DP}$ subunit in their nomenclature) has been suggested to be the active one, in that a water molecule that would carry out nucleophilic attack on the γ-phosphate of ATP during hydrolysis is better positioned than in the other filled site on the $β_{TP}$ subunit. With the empty site as a reference, $β_{DP}$ corresponds to our ADP·Pi and $β_{TP}$ to ATP in Figure 1B (or 1C) iv, in harmony with our reaction scheme.

At low [ATP] around μM where the overall hydrolysis reaction is slow, or under the conditions where ATP synthesis proceeds slowly, many cycles of ATP cleavage and synthesis occur on F_1 before the overall reaction proceeds to a next round: synthesis/hydrolysis in the catalytic site is fully reversible, or ATP and ADP·Pi are near equilibrium (Boyer, 1993). In Figure 1C, this would take place in the state ADP·Pi, if the equilibrium there allows occasional synthesis. In Figure 1B, the ATP at the 120° position (red in i') may occasionally be converted to ADP·Pi for a short moment. The latter is consistent with our recent observation (Shimabukuro et al., 2006) that, when an ATP-waiting dwell is long, the red ATP in i' is hydrolyzed before the cyan ATP binds: if Pi happens to be released upon one of the momentary cleavage events, ATP cannot be reformed and ADP stays.

At yet lower [ATP], ADP is spontaneously released in an ATP-waiting angle and γ often goes back by 40°. The backward rotation presumably diminishes the affinity for ATP of the site that was to bind the next ATP. Thus, F_1 cannot easily resume the normal reaction pathway, unless helped by magnets, and lingers on side paths. Overall, however, the rotation still goes in the correct direction.

Energetics of Coupling
Our view of the coupling between chemical reactions and mechanical work is continual induced fits (Koshland, 1958) and induced 'unfits.' In the case of F_1-ATPase, ATP binding induces the catalytic site into a conformation that better fits ATP, which in turn drives the first 80° conformational change in the whole F_1. After the conformational change, the affinity for ATP should be higher because of the induced fit. During synthesis, ATP that is synthesized but tightly bound to the catalytic site will be released into the medium when γ is rotated in reverse (Yasuda et al., 2001).

Likewise, Pi release renders the site unfit for Pi, thereby driving the second 40° conformational change of F_1. Here we have gone beyond the logic and have shown experimentally that the 40° rotation indeed reduces the affinity for Pi: Boyer's binding change mechanism (Boyer, 1993)

has now been directly proved for this part. Energy-requiring reverse rotation should increase the affinity for Pi, a necessary step in synthesis.

The vertical difference of $\sim 6\,k_{\mathrm{B}}T$ between the two magenta bars in Figure 3A is the conformational (free) energy that can be used to do work during $80° \rightarrow 120°$ rotation, or the work required to let γ rotate in reverse. This energy diagram also reveals how the coupling between chemical reaction and mechanical rotation is ensured. Because forward $80° \rightarrow 120°$ rotation is uphill in the $F_1 \cdot ADP \cdot Pi$ state, forward rotation necessarily accompanies Pi release: γ may thermally rotate forward in the $F_1 \cdot ADP \cdot Pi$ state, but it will come back unless Pi is released. In $120° \rightarrow 80°$ rotation for synthesis, $F_1 \cdot ADP$ state (magenta) poses an uphill that presumably rises more sharply beyond $80°$. Unless Pi is bound and the state changes to green, further backward rotation will be prohibited.

ADP release likely accompanies induced unfit, too. Spontaneous Cy3-ADP release at the ATP-waiting angle of $240°$ takes $\sim 10^1$ s, whereas release is complete in the next $80°$ substep which takes < 33 ms. Forward rotation must increase $k_{\mathrm{off}}^{\mathrm{Cy3-ADP}}$, as evidenced by the acceleration by magnets. Unless $k_{\mathrm{on}}^{\mathrm{Cy3-ADP}}$ increases by the same amount, which is unlikely, the affinity for Cy3-ADP will decrease. Quantitative data on unlabeled ADP is yet unavailable, but it is likely that the affinity for ADP also decreases in the substep from $240°$ to $320°$. If so, it implies that $80°$ substeps are powered by ADP release in addition to ATP binding, as opposed to our original contention (Kinosita et al., 2004; Yasuda et al., 2001) that ATP binding alone drives the $80°$ step. The forward bead displacements simultaneous with Cy3-ADP release in Figure 7 support the new view and further suggest, as already mentioned, that forward torque produced by ADP release begins to operate after γ has rotated beyond the ATP-waiting angle, normally after ATP binding has initiated the $80°$ rotation.

We have proposed that cleavage of ATP may also accompany a small amount of rotation, e.g., $10°$ (Kinosita et al., 2004). Substep amplitudes close to $80°$ have been observed in cases of slow ATP cleavage, leaving the possibility that Pi release drives rotation from $\sim 90°$ to $120°$; high-speed imaging (Figure 2) cannot reliably discriminate $80°$ and $90°$. Coupling between ATP cleavage and rotation will ensure efficient synthesis, because reverse rotation will drive the equilibrium between ATP and $ADP \cdot Pi$ toward synthesis. See-saw energy diagrams as in Figure 3A likely apply to all reactions, binding and release of ATP, ADP, and Pi as well as cleavage/synthesis of ATP. All will then accompany induced fits or unfits, providing basis for efficient coupling.

EXPERIMENTAL PROCEDURES

Proteins

F_1 was biotinylated at the sole two cysteines on γ (Yasuda et al., 2001), and streptavidin conjugated (Yasuda et al., 1998). The β-E190D mutant was purified and biotinylated as described (Shimabukuro et al., 2003). The samples were flash-frozen in liquid nitrogen and stored at $-80°C$ until use.

Flow Chamber

We made two 6-mm wide flow chambers side by side on a 32 × 24 mm² coverslip, functionalized with Ni-NTA (Itoh et al., 2004), by placing three spacers ~ 50-μm thick and an uncoated coverslip (18 × 18 mm²) on top. We infused one chamber volume (~ 5 μl) of 40 pM biotinylated F_1 in buffer A (25 mM MOPS-KOH, 50 mM KCl, 4 mM MgCl₂, [pH 7.0]), waited for 2 min, and infused 20 μl of buffer A and 20 μl of 5 mg/ml BSA in buffer A. We then infused 10 μl of streptavidin-coated magnetic beads (MG-SA with very high biotin binding capacity, nominal diameter 0.711 μm, Seradyn) from which particles $>\sim 0.5$ μm had been removed by centrifugation. After 30 min, we infused 20 μl of buffer A, and then 20 μl of 2.5 mg/ml biotin-labeled BSA (Sigma-Aldrich) to block the surface of magnetic beads. Finally, we infused twice 20 μl of buffer B (buffer A with KCl at 25 mM, plus 1.25 mM creatine phosphate and 0.1 mg/ml creatine kinase) with ATP at a desired level. When Cy3-ATP was included, we used buffer B' (buffer B plus 0.5% (v/v) 2-mercaptoethanol, 0.1 mg/ml glucose-oxidase, 30 U/ml catalase, and 2.25 mg/ml glucose).

Samples for gold bead assay were prepared by the same procedure, except that biotinylated F_1, buffer A and magnetic beads above were replaced with streptavidin-conjugated F_1, buffer C (10 mM MOPS-KOH, 100 mM KCl, [pH 7.0]) and biotinylated 40 nm gold beads (Yasuda et al., 2001), respectively, and infusion of biotin-labeled BSA was omitted. Anions were added as potassium salt in buffer B.

Microscopy

Images of 40 nm gold particles were obtained by laser dark-field microscopy (Yasuda et al., 2001) on an inverted microscope (IX70, Olympus) and recorded with a fast-framing charge-coupled device (CCD) camera (HiD-Cam, Nac) at 8000 frames/s. 1-2 mW of 532 nm laser beam (Millennia II, Spectra-Physics) was introduced in the dark-field condenser to illuminate a sample area ~ 10 μm in diameter.

Cy3-ATP was imaged by TIRF microscopy, where the 532 nm laser beam was introduced from below through an objective (Figure 4A). Ordinary TIRF excitation with a single laser beam lacks oscillation along the beam and is unsuited to quantitative fluorescence. We thus illuminated the sample from all directions (Figure 4A): after making the laser beam circularly polarized with a quarter-wave plate, we let it diverge in a cone-surface shape with a diffractive diffuser (D074A, MEMS Optical), which was rotated at 7,000 rpm by a hollow shaft motor to eliminate interference and speckles, and we focused the diverging beam on the back focal plane of the objective (PlanApo 100 × NA 1.4, Olympus; made magnetization-free by custom-order) in the form of a ring at the numerical aperture of 1.365 (± 1%). Laser power before the objective was 0.11 mW in Figure 4 and 0.05–0.07 mW elsewhere, which illuminated a sample area ~ 17 μm in diameter. Fluorescence was imaged with an intensified (VS4-1845, Videoscope) CCD camera (CCD-300T-IFG, Dage-MTI). Images of magnetic beads, illuminated with a halogen lamp, were separated from fluorescence by a dichroic mirror and captured with another camera (CCD-300-RC, Dage-MTI). Fluorescence and bead images were synchronously combined (Multi Viewer MV-24C, FOR-A) and recorded on a Hi8 video tape (EVO-9650, Sony). We analyzed digitized (Video Savant, IO Industries) images using ImageJ (NIH) and in-house plug-ins. Rotary angles were determined from the centroid of bead images (Yasuda et al., 2001).

To rotate magnetic beads, two opposing pairs of electromagnets made of soft iron, each pole 10 mm wide and 10 mm high and the gap between opposing poles of 20 mm, were mounted 18 mm above the sample (Figure 4A). Magnetic field on the specimen was 40-130 Gauss.

Observations were made at $23 \pm 0.1°C$.

Analysis of Phosphate Kinetics

We analyzed the histograms of $80°$ dwells (Figure 3B) as follows. At 2 mM ATP and 0 mM Pi, the $80°$ dwell consists of two reactions, ATP hydrolysis and Pi release. Fit with a sequential reaction scheme (cyan

line in Figure 3B) gave two rate constants, $(8.6 \pm 0.2) \times 10^3 \text{ s}^{-1}$ and $(7.5 \pm 0.1) \times 10^2 \text{ s}^{-1}$, consistent with previous values (Yasuda et al., 2001). In the presence of Pi, Scheme 6 in the main text applies, for which the dwell-time distribution is given by

$$P(t) \propto -2L \exp\{-k_{\text{hyd}}t\} + \left(2k_{\text{hyd}} - k_{\text{off}}^{\text{Pi}} - k_{\text{rebind}}^{\text{Pi}} - k^+ + L\right)$$
$$\times \exp\left\{-\frac{1}{2}(k_{\text{off}}^{\text{Pi}} + k_{\text{rebind}}^{\text{Pi}} + k^+ + L)t\right\} + \left(-2k_{\text{hyd}} + k_{\text{off}}^{\text{Pi}} + k_{\text{rebind}}^{\text{Pi}} + \right.$$
$$\left. k^+ + L\right)\exp\left\{-\frac{1}{2}(k_{\text{off}}^{\text{Pi}} + k_{\text{rebind}}^{\text{Pi}} + k^+ - L)t\right\} \qquad (8)$$

where $L = \sqrt{-4k_{\text{off}}^{\text{Pi}}k^+ + (k_{\text{off}}^{\text{Pi}} + k_{\text{rebind}}^{\text{Pi}} + k^+)^2}$ (for $k_{\text{off}}^{\text{Pi}} < k_{\text{rebind}}^{\text{Pi}}$). Global fit (magenta lines) to all histograms at 20 μM ATP at various [Pi] in Figure 3B, with all parameters in common except for $k_{\text{rebind}}^{\text{Pi}}(80°)$, gave the results in the main text (Origin software, Origin Lab). The $k_{\text{hyd}}(80°)$ and $k_{\text{off}}^{\text{Pi}}(80°)$ obtained in the global fit agree with the independent analysis at 2mM ATP and 0 mM Pi above.

The analysis of 120° dwells was made as follows. The Scheme 7 in the main text implies that the dwells at 120° terminated by a backward 40° substep (Pi rebinding) and those terminated by a 80° forward substep (ATP binding) should both be distributed as

$$P(t) \propto \exp\{-(k_{\text{on}}^{\text{Pi,app}} \cdot [\text{Pi}] + k_{\text{on}}^{\text{ATP}} \cdot [\text{ATP}])t\} \qquad (9)$$

where

$$k_{\text{on}}^{\text{Pi,app}} = k_{\text{on}}^{\text{Pi}}(120°) \times k^-(\text{F}_1 \cdot \text{ADP} \cdot \text{Pi})/\{k^-(\text{F}_1 \cdot \text{ADP} \cdot \text{Pi}) + k_{\text{off}}^{\text{Pi}}(120°)\} \qquad (10)$$

is the apparent rate of Pi binding (below saturating [Pi]) and $k_{\text{on}}^{\text{ATP}}(120°)$ the apparent rate of ATP binding which we do not distinguish from the true rate. Experimental histograms for the two sets of dwells were indeed exponential with a similar time constant (Figure 3D). We therefore fitted the combined dwells (light gray) with exp(-kt) (green lines) to obtain $k = k_{\text{on}}^{\text{Pi,app}}[\text{Pi}] + k_{\text{on}}^{\text{ATP}}[\text{ATP}]$. In Figure 3E we plot k/[Pi] versus [ATP] (black symbols). The intercept at 0 mM ATP gives $k_{\text{on}}^{\text{Pi,app}} = (4.4 \pm 2.5) \times 10^1 \text{ M}^{-1}\text{s}^{-1}$. Plot of k/[ATP] versus [Pi] (black in Figure 3F) gives $k_{\text{on}}^{\text{ATP}}(120°) = (1.7 \pm 0.4) \times 10^7 \text{ M}^{-1}\text{s}^{-1}$. A caveat here is that the substrate of F$_1$-ATPase is MgATP (Weber et al., 1994) whereas Mg is chelated by Pi. When we use corrected [MgATP] (gray symbols) instead of added [ATP], we obtain

$$k_{\text{on}}^{\text{Pi,app}} = (4.4 \pm 2.5) \times 10^1 \text{M}^{-1}\text{s}^{-1} \qquad (11)$$

and $k_{\text{on}}^{\text{ATP}}(120°) = (2.0 \pm 0.3) \times 10^7 \text{ M}^{-1}\text{s}^{-1}$. These latter values do not differ significantly from the values without correction, because $k_{\text{on}}^{\text{Pi,app}}$ and $k_{\text{on}}^{\text{ATP}}(120°)$ are estimated at the limit of [ATP]→0 and [Pi]→0, respectively.

Putting $K_{\text{d}}^{\text{Pi}}(80°) = 4.9$ mM and $k^+(\text{F}_1 \cdot \text{ADP})/k^-(\text{F}_1 \cdot \text{ADP}) = 450$ into Equation 5, we obtain

$$K_{\text{d}}^{\text{Pi}}(120°) \times \{k^+(\text{F}_1 \cdot \text{ADP} \cdot \text{Pi})/k^-(\text{F}_1 \cdot \text{ADP} \cdot \text{Pi})\} = 2.2 \text{ M} \qquad (12)$$

Because the backward 40° substep was as fast as the forward substep, we set

$$k^-(\text{F}_1 \cdot \text{ADP} \cdot \text{Pi}) \approx 10^4 \text{s}^{-1} \qquad (13)$$

Further analysis to obtain parameter values in Equation 12 is split into two alternative branches. (i) If $k^-(\text{F}_1 \cdot \text{ADP} \cdot \text{Pi}) < k_{\text{off}}^{\text{Pi}}(120°)$, then Equation 10 becomes

$$k_{\text{on}}^{\text{Pi,app}} \approx k^-(\text{F}_1 \cdot \text{ADP} \cdot \text{Pi})/K_{\text{d}}^{\text{Pi}}(120°) = 44 \text{ M}^{-1}\text{s}^{-1} \qquad (14)$$

where the numerical value is from Equation 11. Equation 12 then reads $k^+(\text{F}_1 \cdot \text{ADP} \cdot \text{Pi}) \approx 10^2 \text{ s}^{-1}$. From Equation 12, then, we obtain $K_{\text{d}}^{\text{Pi}}(120°) \approx 2 \times 10^2$ M. Since the assumption for this branch is $k_{\text{off}}^{\text{Pi}}(120°) > k^-(\text{F}_1 \cdot \text{ADP} \cdot \text{Pi}) \approx 10^4 \text{ s}^{-1}$ and since Equation 10 dictates $k_{\text{on}}^{\text{Pi}}(120°) > k_{\text{on}}^{\text{Pi,app}}$, we make an arbitrary choice of $k_{\text{off}}^{\text{Pi}}(120°) = 10^7 \text{ s}^{-1}$ and $k_{\text{on}}^{\text{Pi}}(120°) = 5 \times 10^4 \text{ M}^{-1}\text{s}^{-1}$.

(ii) If $k^-(\text{F}_1 \cdot \text{ADP} \cdot \text{Pi}) > k_{\text{off}}^{\text{Pi}}(120°)$, then Equations 10 and 11 lead to

$$k_{\text{on}}^{\text{Pi,app}} \approx k_{\text{on}}^{\text{Pi}}(120°) = 44 \text{ M}^{-1}\text{s}^{-1} \qquad (15)$$

Putting Equations 13 and 15 into Equation 12, we obtain

$$k_{\text{off}}^{\text{Pi}}(120°) \times k^+(\text{F}_1 \cdot \text{ADP} \cdot \text{Pi}) = 1 \times 10^6 \text{ s}^{-2} \qquad (16)$$

The rate of forward rotation without Pi release, $k^+(\text{F}_1 \cdot \text{ADP} \cdot \text{Pi})$, must be $< 10^3 \text{ s}^{-1}$ because the 80° dwell is ~2 ms, and the assumption for branch (ii) is $k_{\text{off}}^{\text{Pi}}(120°) < k^-(\text{F}_1 \cdot \text{ADP} \cdot \text{Pi}) \approx 10^4 \text{ s}^{-1}$. The slim choice that is left for Equation 16 is $k^+(\text{F}_1 \cdot \text{ADP} \cdot \text{Pi}) \approx 3 \times 10^2 \text{ s}^{-1}$, $k_{\text{off}}^{\text{Pi}}(120°) \approx 3 \times 10^3 \text{ s}^{-1}$. With Equation 15, $K_{\text{d}}^{\text{Pi}}(120°) \approx 70$ M.

Calibrations

Fluorescence intensity of a single Cy3-ATP on F$_1$ was determined in a mixture of 100 nM Cy3-ATP and 200 nM unlabeled ATP, where at most one Cy3-ATP would bind to F$_1$ at any moments. From 32 binding events in four F$_1$ molecules during rotation without magnets, we obtained an average intensity, above background, of 12.1 ± 0.3 arbitrary unit (au), consistent with the quantized intensities in Figure 6D. The background intensity varied with [Cy3-ATP], and is shown as "0" in Figures 5–7. We also confirmed that we could resolve up to three Cy3 molecules bound to F$_1$. For this, we used β-F420C mutant that has a cysteine residue on each β at the entrance of nucleotide binding pocket. We moderately labeled it with Cy3-monofunctional maleimide. Spot intensities of the labeled mutant had three major peaks at multiples of 14.4 au, equivalent with 13.1 au of bound Cy3-ATP (calibration in a fluorometer).

The rate of photobleaching of Cy3 was also measured on this labeled mutant under conditions similar to Figures 5–7. The time to photobleaching distributed exponentially with a time constant of 56 ± 7 s (n = 400). 6%–7% showed frequent blinking, once in several seconds on average and lasting ~1 s or less, and 1%–2% blinked once or twice before photobleaching. The rest did not blink. The reason for the heterogeneity is unknown. The case of frequent blinking was less noticeable with Cy3-ATP.

Ionic strengths in Figures 2E and 2F were calculated as $1/2 \cdot \sum (c_i z_i^2)$, where c_i is the concentration and z_i charge number of ith ion. Phosphate and succinate concentrations were estimated by solving Henderson-Hasselbalch equation, $pH = pK_2 - \log(\gamma_1/\gamma_2) + \log([A^{2-}]/[HA^{1-}])$, where $pH = 7.0$ and for phosphate (Cohn, 1927), $pK_2 = 7.16$, $\log(\gamma_1/\gamma_2) = 0.35$ (50 mM), 0.473 (200 mM), and 0.545 (500 mM); for succinate (Esteso et al., 1987), $pK_2 = 5.57$ and $\log(\gamma_1/\gamma_2) = 0.587$ (50 mM), 0.4877 (200 mM), 0.4615 (500 mM).

Corrected [MgATP] in Figures 3E and 3F was calculated from [MgATP] = K_{ATP} [ATP] [Mg] and [MgPi] = K_{Pi} [Pi] [Mg], where K_{ATP} and K_{Pi} are $10^{4.6}$ and $10^{2.9}$ (Sillén and Martell, 1964); [Mg] = [added Mg] – [MgATP] – [MgPi]; [ATP] = [added ATP] – [MgATP]; [Pi] = [added Pi] – [MgPi].

REFERENCES

Abrahams, J.P., Leslie, A.G.W., Lutter, R., and Walker, J.E. (1994). Structure at 2.8 Å resolution of F_1-ATPase from bovine heart mitochondria. Nature 370, 621–628.

Adachi, K., Yasuda, R., Noji, H., Itoh, H., Harada, Y., Yoshida, M., and Kinosita, K., Jr. (2000). Stepping rotation of F_1-ATPase visualized through angle-resolved single-fluorophore imaging. Proc. Natl. Acad. Sci. USA 97, 7243–7247.

Al-Shawi, M.K., Ketchum, C.J., and Nakamoto, R.K. (1997). The *Escherichia coli* F_OF_1 γM23K uncoupling mutant has a higher $K_{0.5}$ for Pi. Transition state analysis of this mutant and others reveals that synthesis and hydrolysis utilize the same kinetic pathway. Biochemistry 36, 12961–12969.

Boyer, P.D. (1993). The binding change mechanism for ATP synthase - some probabilities and possibilities. Biochim. Biophys. Acta 1140, 215–250.

Boyer, P.D., and Kohlbrenner, W.E. (1981). The present status of the binding-change mechanism and its relation to ATP formation by chloroplasts. In Energy Coupling in Photosynthesis, B.R. Selman and S. Selman-Reimer, eds. (Amsterdam: Elsevier), pp. 231–240.

Cohn, E.J. (1927). The activity coefficients of the ions in certain phosphate solutions a contribution to the theory of buffer action. J. Am. Chem. Soc. 49, 173–193.

De La Cruz, E.M., and Ostap, E.M. (2004). Relating biochemistry and function in the myosin superfamily. Curr. Opin. Cell Biol. 16, 61–67.

Esteso, M.A., Fernandez-Merida, L., and Hernandez-Luis, F.F. (1987). Activity coefficients for aqueous Na_2Succ solutions from emf measurements. J. Electroanal. Chem. 230, 69–75.

Funatsu, T., Harada, Y., Tokunaga, M., Saito, K., and Yanagida, T. (1995). Imaging of single fluorescent molecules and individual ATP turnovers by single myosin molecules in aqueous solution. Nature 374, 555–559.

Hirono-Hara, Y., Noji, H., Nishiura, M., Muneyuki, E., Hara, K.Y., Yasuda, R., Kinosita, K., Jr., and Yoshida, M. (2001). Pause and rotation of F_1-ATPase during catalysis. Proc. Natl. Acad. Sci. USA 98, 13649–13654.

Itoh, H., Takahashi, A., Adachi, K., Noji, H., Yasuda, R., Yoshida, M., and Kinosita, K., Jr. (2004). Mechanically driven ATP synthesis by F_1-ATPase. Nature 427, 465–468.

Kabaleeswaran, V., Puri, N., Walker, J.E., Leslie, A.G.W., and Mueller, D.M. (2006). Novel features of the rotary catalytic mechanism revealed in the structure of yeast F_1 ATPase. EMBO J. 25, 5433–5442.

Kagawa, R., Montgomery, M.G., Braig, K., Leslie, A.G.W., and Walker, J.E. (2004). The structure of bovine F_1-ATPase inhibited by ADP and beryllium fluoride. EMBO J. 23, 2734–2744.

Kinosita, K., Jr., Adachi, K., and Itoh, H. (2004). Rotation of F_1-ATPase: how an ATP-driven molecular machine may work. Annu. Rev. Biophys. Biomol. Struct. 33, 245–268.

Kinosita, K., Jr., Yasuda, R., Noji, H., and Adachi, K. (2000). A rotary molecular motor that can work at near 100% efficiency. Philos. Trans. R. Soc. Lond. B Biol. Sci. 355, 473–489.

Koshland, D.E. (1958). Application of a theory of enzyme specificity to protein synthesis. Proc. Natl. Acad. Sci. USA 44, 98–104.

Masaike, T., Muneyuki, E., Noji, H., Kinosita, K., Jr., and Yoshida, M. (2002). F_1-ATPase changes its conformations upon phosphate release. J. Biol. Chem. 277, 21643–21649.

Menz, R.I., Walker, J.E., and Leslie, A.G.W. (2001). Structure of bovine mitochondrial F_1-ATPase with nucleotide bound to all three catalytic sites: implications for the mechanism of rotary catalysis. Cell 106, 331–341.

Nishizaka, T., Oiwa, K., Noji, H., Kimura, S., Muneyuki, E., Yoshida, M., and Kinosita, K., Jr. (2004). Chemomechanical coupling in F_1-ATPase revealed by simultaneous observation of nucleotide kinetics and rotation. Nat. Struct. Mol. Biol. 11, 142–148.

Noji, H., Yasuda, R., Yoshida, M., and Kinosita, K., Jr. (1997). Direct observation of the rotation of F_1-ATPase. Nature 386, 299–302.

Oiwa, K., Jameson, D.M., Croney, J.C., Davis, C.T., Eccleston, J.F., and Anson, M. (2003). The 2′-O- and 3′-O-Cy3-EDA-ATP(ADP) complexes with myosin subfragment-1 are spectroscopically distinct. Biophys. J. 84, 634–642.

Sakaki, N., Shimo-Kon, R., Adachi, K., Itoh, H., Furuike, S., Muneyuki, E., Yoshida, M., and Kinosita, K., Jr. (2005). One rotary mechanism for F_1-ATPase over ATP concentrations from millimolar down to nanomolar. Biophys. J. 88, 2047–2056.

Shimabukuro, K., Muneyuki, E., and Yoshida, M. (2006). An alternative reaction pathway of F_1-ATPase suggested by rotation without 80°/40° substeps of a sluggish mutant at low ATP. Biophys. J. 90, 1028–1032.

Shimabukuro, K., Yasuda, R., Muneyuki, E., Hara, K.Y., Kinosita, K., Jr., and Yoshida, M. (2003). Catalysis and rotation of F_1 motor: cleavage of ATP at the catalytic site occurs in 1 ms before 40° substep rotation. Proc. Natl. Acad. Sci. USA 100, 14731–14736.

Sillén, L.G., and Martell, A.E. (1964). Stability constants of metal-ion complexes, Spec. Publ. 17 (London: The Chemical Society).

Weber, J., and Senior, A.E. (2000). ATP synthase: what we know about ATP hydrolysis and what we do not know about ATP synthesis. Biochim. Biophys. Acta 1458, 300–309.

Weber, J., Wilke-Mounts, S., and Senior, A.E. (1994). Cooperativity and stoichiometry of substrate binding to the catalytic sites of *Escherichia coli* F_1-ATPase. Effects of magnesium, inhibitors, and mutation. J. Biol. Chem. 269, 20462–20467.

Yasuda, R., Masaike, T., Adachi, K., Noji, H., Itoh, H., and Kinosita, K., Jr. (2003). The ATP-waiting conformation of rotating F_1-ATPase revealed by single-pair fluorescence resonance energy transfer. Proc. Natl. Acad. Sci. USA 100, 9314–9318.

Yasuda, R., Noji, H., Kinosita, K., Jr., and Yoshida, M. (1998). F_1-ATPase is a highly efficient molecular motor that rotates with discrete 120° steps. Cell 93, 1117–1124.

Yasuda, R., Noji, H., Yoshida, M., Kinosita, K., Jr., and Itoh, H. (2001). Resolution of distinct rotational substeps by submillisecond kinetic analysis of F_1-ATPase. Nature 410, 898–904.

Yoshida, M., Muneyuki, E., and Hisabori, T. (2001). ATP synthase — a marvellous rotary engine of the cell. Nat. Rev. Mol. Cell Biol. 2, 669–677.